Ecological Forest Management Handbook

Second Edition

Edited by Guy R. Larocque

Second edition published 2025

ISBN: 978-1-032-55517-1 (hbk)
ISBN: 978-1-032-55518-8 (pbk)
ISBN: 978-1-003-43108-4 (ebk)

18 Application of Surface Modeling for Large Regions

A Case Study for Forest Carbon Stocks in China

Tian-Xiang Yue, Yi-Fu Wang, and Guy R. Larocque

DOI: 10.1201/9781003431084-22

CRC Press
Taylor & Francis Group
Boca Raton London New York

CRC Press is an imprint of the
Taylor & Francis Group, an **informa** business

18 Application of Surface Modeling for Large Regions
A Case Study for Forest Carbon Stocks in China

Tian-Xiang Yue, Yi-Fu Wang, and Guy R. Larocque

18.1 INTRODUCTION

Surface modeling refers to the process of simulating a surface by efficiently combining satellite remotely sensed data with ground-based observation data, such as a scattered point-form dataset, a line-form dataset and/or an area-form dataset. Surface modeling formulates an object in a grid system (Yue 2011). Each grid cell includes an estimate of the object that represents the characteristics for that particular location. There are four advantages to represent data in grid form (Martin and Bracken 1991; Deichmann 1996; Yue et al. 2008; 2009, 2010a, 2010b): (1) a regular grid can be easily regrouped into any new aerial arrangement; (2) ecological data organized in a grid form can facilitate compatibility among heterogeneous datasets; (3) multiresolution and multisource information can be amalgamated more easily when data are in a grid form, and (4) some of the problems caused by different types of boundaries may be avoided when data are converted into a grid form.

Surface modeling began to be used effectively in the 1960s when computers became more accessible (Lo and Yeung 2002). However, its development was limited until the 1990s because of the limited computational capacity of computers. The application of surface modeling requires powerful software and large storage capacities to handle spatially explicit data over large regions. Significant advances in surface modeling were intimately associated with developments in several areas, including trend surface analysis (TSA) (Ahlberg et al. 1967; Schroeder and Sjoquist 1976; Legendre and Legendre 1983), digital terrain modeling (Stott 1977), surface approximation (Long 1980), spatial simulation of wetland habitats (Sklar et al. 1985), spatial pattern matching (Costanza 1989), spatial prediction (Turner et al. 1989), and modeling of coastal landscape dynamics (Costanza et al. 1990). Technological advances in remote sensing (RS) and geographic information systems (GIS) and the accumulation of spatially explicit data have contributed to the extensive development and application of surface modeling to analyze and understand the spatial phenomena of ecological processes for the last three decades (Yue 2011). Landmark case examples can be found in Sklar et al. (1985) for the spatial simulation model of habitat changes in relation to marsh type, hydrology, subsidence, and sediment transport for a generalized coastal wetland area, Turner et al. (1989) for the comparison of spatial patterns and Costanza and Maxwell (1991) for application on workstations.

Then, methodological developments continued on several fronts, such as the simulation of ecosystems with spatial heterogeneity (Gao 1996), a pairwise potential modeling approach (Reich et al.

DOI: 10.1201/9781003431084-22

1997), a patch-based spatial modeling approach to analyze the effects of spatial heterogeneity on ecological processes (Wu and Levin 1997), a daily high-resolution weather generator (Friend 1998), and a GIS-based spatial modeling method for the simulation of the geographic distribution of wildlife populations (Ji and Jeske 2000). The global carbon cycle was examined using different surface models that were sensitive to spatial distributions of productivity, biomass, and soil organic matter (Haxeltine and Prentice 1996; Svirezhev 2002). Perry and Enright (2002) developed a spatially explicit grid-based model to examine the extent to which past and future modifications in disturbance regimes may affect landscape structure.

The surface modeling method in forestry applications has embodied the forest properties and parameters of surface simulation. The classical method for obtaining forest attributes and parameters includes forest resources surveys in which population estimates are derived using samples. The measured data from forest resources survey form a point-form dataset. However, forest attributes and parameters (e.g., forest type, stock volume, biomass, and carbon storage) should be expressed as grid or raster data to explain the distribution. Surface modeling is an efficient approach to convert point-form data into grid data and consists of an appropriate method to simulate the distribution of forest attributes and parameters based on different data amalgamations that may originate from remote sensing observations and ground-based observation data.

In this chapter, some methods of earth surface modeling are briefly introduced, with a focus on the method used for high accuracy surface modeling (YUE-HASM). For more details, readers are encouraged to consult Yue (2011) for a complete introduction on the subject. A case study of the application of surface modeling to quantify carbon stocks in China is presented.

18.2 METHODS OF SURFACE MODELING

18.2.1 Trend Surface Analysis

Trend surface analysis uses least-squares regression to fit a trend surface from sparse data that consist of spatial coordinates. Good approximations can be obtained when the trend surface is formulated as a "n" order polynomial surface:

$$z(x,y) = \sum_{i=0}^{n} \sum_{j=0}^{n-i} a_{i,j} \cdot x^i \cdot y^j \tag{18.1}$$

Where $z(x,y)$ is the value of the trend surface at the grid (x, y); x and y are the independent variables; $a_{i,j}(i = 1, \ldots, n; j = 1, \ldots, n)$ are parameters to be simulated; and n is the order of the polynomial surface. There is a major weakness with TSA. Details can be lost because the poor smoothing in some surface regions may affect the fit of other surface regions. Also, TSA assumes that the residuals are independent, but this assumption is violated most of the time, which has consequences on the estimated variance (Oliver and Webster 1990).

18.2.2 Inverse Distance Weighted Method

The inverse distance weighted method (IDW) can be formulated as (Shepard 1968)

$$z_{i,j} = \left(\sum_{k=1}^{m_{i,j}} \frac{1}{\left(d_{i,j,k}\right)^a} \right)^{-1} \sum_{k=1}^{m_{i,j}} \frac{z_k}{\left(d_{i,j,k}\right)^a} \tag{18.2}$$

where, $z_{i,j}$ indicates the estimate made at the location (i, j) for which an estimate is required because of the absence of measurements. The estimates are computed from the $m_{i,j}$ neighbor observations;

z_k is the k_{th} neighbor observation; $d_{i,j,k}$ is the distance from z_k to (i, j); and a is the parameter to be determined. The main shortcoming of IDW is the inability to integrate the spatial structure and information beyond the neighborhood (Zhao et al. 2005, Magnussen et al. 2007).

18.2.3 Triangulated Irregular Network

The triangulated irregular network (TIN) method is well recognized to represent surface models in GIS (Bengtsson and Nordbeck 1964), as it supports a simple data structure and can easily be rendered using common graphics hardware (Yang et al. 2000). TIN is composed of nodes, edges, triangles, topological information, and a hull. This method is based on linear interpolation in a triangulated irregular network and is used to fit irregularly distributed points into a surface of each triangle. It is one of the basic models used to represent digital terrain pieces of land on the Earth's surface (Tse and Gold 2004).

Even though TIN models of the terrain surface are well known in GIS, their main shortcoming is that they ignore nonlinear information and are unable to represent cliffs, caves, or holes (Tse and Gold 2004).

18.2.4 Kriging

Kriging, named after the South African mining engineer D.G. Krige (Kleijnen and van Beers 2005), is the term used for a family of generalized linear least-squares regression algorithms that interpolate values in a random field for unobserved locations using observations from neighborhood locations (Krige 1951). Considered as a fundamental method in geostatistics, Kriging includes ordinary kriging (OK), co-kriging, and disjunctive kriging (Kleijnen 2009).

18.2.5 Spline

There are different types of spline: uniform rational basis-spline, uniform non-rational basis-spline, non-uniform-non-rational basis-spline, and non-uniform rational basis-spline. These different methods are based on the basis-spline, which includes cubic polynomial regressions with any number of curve segments (Watt 2000). Each curve segment has four control points and each control point influences four curve segments, which is the local control property of the basis-spline curve. The entire set of curve segments, $Q(u)$, is defined as one basis-spline curve

$$Q(u) = \sum_{i=0}^{m} P_i \cdot B_i(u) \tag{18.3}$$

where i is a nonlocal control point number; u is a global parameter; P_i is the ith control point; m is total number of the control points; and $B_i(u)$ is the ith basis-spline.

18.2.6 YUE-HASM

The method used for high accuracy surface modeling (YUE-HASM) is a more complex approach than the previous ones. When the surface can be represented as $z = (x, y, f(x, y))$, then the first fundamental coefficients can be formulated as:

$$\begin{cases} E = 1 + f_x^2 \\ F = f_x f_y \\ G = 1 + f_y^2 \end{cases} \tag{18.4}$$

The second fundamental coefficients can be formulated as:

$$\begin{cases} L = \dfrac{f_{xx}}{\sqrt{1+f_x^{\,2}+f_y^{\,2}}} \\ M = \dfrac{f_{xy}}{\sqrt{1+f_x^{\,2}+f_y^{\,2}}} \\ N = \dfrac{f_{yy}}{\sqrt{1+f_x^{\,2}+f_y^{\,2}}} \end{cases} \tag{18.5}$$

These two coefficient sets must satisfy the following Gauss equation set,

$$\begin{cases} f_{xx} = \Gamma_{11}^{1} f_x + \Gamma_{11}^{2} f_y + \dfrac{L}{\sqrt{E+G-1}} \\ f_{xy} = \Gamma_{12}^{1} f_x + \Gamma_{12}^{2} f_y + \dfrac{M}{\sqrt{E+G-1}} \\ f_{yy} = \Gamma_{22}^{1} f_x + \Gamma_{22}^{2} f_y + \dfrac{N}{\sqrt{E+G-1}} \end{cases} \tag{18.6}$$

where $\Gamma_{11}^{1} = \dfrac{GE_x - 2FF_x + FE_y}{2(EG-F^2)}$, $\Gamma_{12}^{1} = \dfrac{GE_y - FG_x}{2(EG-F^2)}$, $\Gamma_{22}^{1} = \dfrac{2GF_y - GG_x - FG_y}{2(EG-F^2)}$, $\Gamma_{11}^{2} = \dfrac{2EF_x - EE_y - FE_x}{2(EG-F^2)}$, $\Gamma_{12}^{2} = \dfrac{EG_x - FE_y}{2(EG-F^2)}$ and $\Gamma_{22}^{2} = \dfrac{EG_y - 2FF_y + FG_x}{2(EG-F^2)}$ are the second kind of Christoffel symbols.

If $\left\{\left(x_i, y_j\right)\right\}$ is an orthogonal division of a computational domain and h the simulation step length, the central point of lattice $(x_{\mathrm{i}}, y_{\mathrm{j}})$ could be expressed as $(0.5h+(i-1)h, 0.5h+(j-1)h)$, where $i = 0,1,2,...,I,I+1$ and $j = 0,1,2,...,J,J+1$. If $f_{\mathrm{i,j}}^{(n)}$ $(n \geq 0)$ represents the iterants of $f(x,y)$ at $(x_{\mathrm{i}}, y_{\mathrm{j}})$ in the nth iterative step, the interpolations are represented by $\left\{f_{\mathrm{i,j}}^{(0)}\right\}$ based on sampling values $\left\{\overline{f}_{\mathrm{i,j}}\right\}$. In terms of numerical mathematics (Quarteroni et al. 2000), the iterative formulation of the YUE-HASM master equation set can be expressed as (Yue et al.,2013b; Zhao and Yue 2014),

$$\begin{aligned} &\frac{-f_{i+2,j}^{(n+1)} + 16f_{i+1,j}^{(n+1)} - 30f_{i,j}^{(n+1)} + 16f_{i-1,j}^{(n+1)} - f_{i-2,j}^{(n+1)}}{12h^2} \\ &= \left(\Gamma_{11}^{1}\right)_{i,j}^{(n)} \frac{f_{i+1,j}^{(n)} - f_{i-1,j}^{(n)}}{2h} + \left(\Gamma_{11}^{2}\right)_{i,j}^{(n)} \frac{f_{i,j+1}^{(n)} - f_{i,j-1}^{(n)}}{2h} + \frac{L_{ij}^{(n)}}{\sqrt{E_{i,j}^{(n)} + G_{i,j}^{(n)} - 1}} \end{aligned} \tag{18.7}$$

$$\begin{aligned} &\frac{-f_{i,j+2}^{(n+1)} + 16f_{i,j+1}^{(n+1)} - 30f_{i,j}^{(n+1)} + 16f_{i,j-1}^{(n+1)} - f_{i,j-2}^{(n+1)}}{12h^2} \\ &= \left(\Gamma_{22}^{1}\right)_{i,j}^{(n)} \frac{f_{i+1,j}^{(n)} - f_{i-1,j}^{(n)}}{2h} + \left(\Gamma_{22}^{2}\right)_{i,j}^{(n)} \frac{f_{i,j+1}^{(n)} - f_{i,j-1}^{(n)}}{2h} + \frac{N_{ij}^{(n)}}{\sqrt{E_{i,j}^{(n)} + G_{i,j}^{(n)} - 1}} \end{aligned} \tag{18.8}$$

$$\frac{f_{i+1,j+1}^{(n+1)} - f_{i+1,j}^{(n+1)} - f_{i,j+1}^{(n+1)} + 2f_{i,j}^{(n+1)} + f_{i-1,j}^{(n+1)} - f_{i,j-1}^{(n+1)} + f_{i-1,j-1}^{(n+1)}}{2h^2}$$

$$= \left(\Gamma_{12}^{1}\right)_{i,j}^{(n)} \frac{f_{i+1,j}^{(n)} - f_{i-1,j}^{(n)}}{2h} + \left(\Gamma_{12}^{2}\right)_{i,j}^{(n)} \frac{f_{i,j+1}^{(n)} - f_{i,j-1}^{(n)}}{2h} + \frac{M_{ij}^{(n)}}{\sqrt{E_{i,j}^{(n)} + G_{i,j}^{(n)} - 1}} \tag{18.9}$$

where $E_{\mathrm{i,j}}^{(n)}$, $F_{\mathrm{i,j}}^{(n)}$ and $G_{\mathrm{i,j}}^{(n)}$ are the iterants of the first fundamental coefficients at the nth iterative step; $L_{\mathrm{i,j}}^{(n)}$, $M_{\mathrm{i,j}}^{(\mathrm{n})}$ and $N_{\mathrm{i,j}}^{(n)}$ represent the iterants of the second fundamental coefficients at the nth iterative step; $(\Gamma_{11}^{1})_{i,j}^{(n)}$, $(\Gamma_{11}^{2})_{i,j}^{(n)}$, $(\Gamma_{22}^{1})_{i,j}^{(n)}$ and $(\Gamma_{22}^{2})_{i,j}^{(n)}$ are the iterants of the Christoffel symbols of the second kind at the nth iterative step, which depend only upon the first fundamental coefficients and their derivatives.

The matrix formulation of YUE-HASM master equations can be respectively expressed as,

$$\mathbf{A} \cdot \mathbf{z}^{(n+1)} = \mathbf{d}^{(n)} \tag{18.10}$$

$$\mathbf{B} \cdot \mathbf{z}^{(n+1)} = \mathbf{q}^{(n)} \tag{18.11}$$

$$\mathbf{C} \cdot \mathbf{z}^{(n+1)} = \mathbf{p}^{(n)} \tag{18.12}$$

where $\mathbf{A}$, $\mathbf{B}$, and $\mathbf{C}$ represent coefficient matrixes of the first equation, the second equation, and the third equation; $\mathbf{d}^{(n)}$, $\mathbf{q}^{(n)}$ and $\mathbf{p}^{(n)}$ are right-hand side vectors of the three equations respectively; $\mathbf{z}^{(n+1)} = \left(f_{1,1}^{(n+1)},...,f_{1,J}^{(n+1)},.....,f_{I,1}^{(n+1)},...,f_{I,J}^{(n+1)}\right)^T = \left(z_1^{(n+1)},...,z_J^{(n+1)},...,z_{(I-1)\cdot J+1}^{(n+1)},...,z_{I\cdot J}^{(n+1)}\right)^T$, $f_{i,j}^{(n)}$ is the value of the nth iteration of $f(x,y)$ at grid cell (x_i, y_i) ; $z_{(i-1)\cdot J+j}^{(n+1)} = f_{i,j}^{(n+1)}$ for $1 \le i \le I$, $1 \le j \le J$.

If $\overline{f}_{i,j}$ is value of $z = f(x,y)$ at the pth sampled point (x_i, y_j), $s_{p,(i-1)\times J+j} = 1$, $k_p = \overline{f}_{i,j}$. There is only one non-zero element, 1, in every row of the coefficient matrix, $\mathbf{S}$, making it a sparse matrix. The solution procedure of YUE-HASM, taking the sampled points as its constraints, can be transformed into solving the following linear equation set in terms of least squares principle.

$$\begin{bmatrix}\mathbf{A}^T & \mathbf{B}^T & \mathbf{C}^T & \lambda\cdot\mathbf{S}^T\end{bmatrix}\begin{bmatrix}\mathbf{A}\\ \mathbf{B}\\ \mathbf{C}\\ \lambda\cdot\mathbf{S}\end{bmatrix}\mathbf{z}^{(n+1)} = \begin{bmatrix}\mathbf{A}^T & \mathbf{B}^T & \mathbf{C}^T & \lambda\cdot\mathbf{S}^T\end{bmatrix}\begin{bmatrix}\mathbf{d}^{(n)}\\ \mathbf{q}^{(n)}\\ \mathbf{p}^{(n)}\\ \lambda\cdot\mathbf{k}\end{bmatrix} \tag{18.13}$$

The parameter λ is the weight of the sampling points and determines the contribution of the sampling points to the simulated surface. λ can be a real number, which means all sampling points have the same weight, or a sector, which means every sampling point has its own weight. An area affected by a sampling point in a complex region is smaller than in a flat region. Therefore, a smaller value of λ is selected in a complex region, and a bigger value of λ is selected in a flat region.

Let

$$\mathbf{W} = \begin{bmatrix}\mathbf{A}^T & \mathbf{B}^T & \mathbf{C}^T & \lambda\cdot\mathbf{S}^T\end{bmatrix}\begin{bmatrix}\mathbf{A}\\ \mathbf{B}\\ \mathbf{C}\\ \lambda\cdot\mathbf{S}\end{bmatrix} \text{ and,}$$

$\mathbf{v}^{(n)} = \begin{bmatrix} \mathbf{A}^T & \mathbf{B}^T & \mathbf{C}^T & \lambda \cdot \mathbf{S}^T \end{bmatrix} \begin{bmatrix} \mathbf{d}^{(n)} \\ \mathbf{q}^{(n)} \\ \mathbf{p}^{(n)} \\ \lambda \cdot \mathbf{k} \end{bmatrix}$, then YUE-HASM has the following formulation:

$$\mathbf{W} \cdot \mathbf{z}^{(n+1)} = \mathbf{v}^{(n)} \tag{18.14}$$

In terms of Gauss-Codazii equation set, iteration stopping criterion of YUE-HASM is formulated as,

$$\begin{gathered} \left(\varphi_{1y} - \phi_{2x} - \varphi_2 P - \phi_1 Q\right)^2 + \\ \left(\varphi_{2x} - \phi_{1y} - \varphi_1 Q - \phi_2 P\right)^2 \\ \left(Q_x + P_y + \varphi_1 \varphi_2 - \phi_1 \phi_2\right)^2 < \mathrm{EI} \end{gathered} \tag{18.15}$$

where $\varphi_1 = \frac{L}{\sqrt{E}}$; $\varphi_2 = \frac{N}{\sqrt{G}}$; $P = \frac{\sqrt{E}_y}{\sqrt{G}}$; $Q = \frac{\sqrt{G}_x}{\sqrt{E}}$; $\phi_1 = \frac{M}{\sqrt{G}}$; $\phi_2 = \frac{M}{\sqrt{E}}$; EI is the iteration stopping criterion of YUE-HASM determined by an application requirement for accuracy.

Many studies described the essential significance of both satellite remotely sensed data and ground-based observation data, but the challenge is how to combine these two kinds of information. YUE-HASM incorporates reinforced machine learning and provides a solution to this challenge (Haber 2021). It can be transformed into a large sparse linear system and combined with the HarrowHassidim-Lloyd (HHL) quantum algorithm to support quantum machine learning (Yue et al. 2022, 2023).

There are several applications of YUE-HASM, including the simulation of climate change (Yue et al. 2013a, 2013b, Zhao and Yue 2014), the development of digital elevation maps (Yue et al. 2007a, 2010a, 2010b, Yue and Wang 2010), and the interpolation of soil properties (Yue 2011, Shi et al. 2009, 2011).

18.3 CASE STUDY: SURFACE MODELING FOR FOREST CARBON STOCKS IN CHINA

By integrating photosynthesis, autotrophic respiration, and litterfall fluxes, biomass dynamics reflects the potential of vegetation to act as a long-term carbon sink (Thurner et al. 2014). Forest ecosystems cover more than 41 million km^2 of the Earth's land area and are thought to contain about half of the carbon in terrestrial biomes (Prentice et al. 2001). Many studies on forest carbon stocks have been conducted in China in recent years.

According to the Integrated Terrestrial Ecosystem C-budget model, China's forests were a source of 21.0 ± 7.8 TgC yr^{-1} from 1901 to 1949 due to human activities. This source increased by 122.3 ± 25.3 TgCyr^{-1} between 1950 and 1987 due to intensified human activities. However, forests became large sinks of 176.7 ± 44.8 TgCyr^{-1} from 1988 to 2001 because of large-scale plantation programs and forest regrowth in previously disturbed areas as well as climatic warming, atmospheric CO_2 fertilization, and N deposition (Wang et al. 2007). The latter factors contributed to increasing forest growth, resulting in more CO_2 uptake. Vegetation carbon sink was defined as carbon sequestration from the atmosphere (1.63 times NPP), vegetation carbon stock as the carbon content that

aboveground vegetation holds, and soil carbon stock as the carbon content that soil organic matter holds. In terms of these definitions, the vegetation carbon stock was 1.58 Pg C and the soil carbon stock was 1.41 Pg C in forest ecosystems of China from 1981 to 2000 (Deng et al. 2011). Forest stands have great potential to sequester more biomass carbon in the future due to large fractions of young and middle-aged forests. According to available national-scale information, mean vegetation carbon in China was 36.98 Pg, and mean soil carbon was 100.75 Pg. Forests had mean vegetation carbon of 5.49 Pg, whereas grasslands had 1.41 Pg (Ni 2013).

According to the continuous biomass expansion factor (BEF) method, based on field measurements of forests plots in different age classes and forest inventory data, carbon density (CD) of the forests in the Pearl River Delta increased by 14.3% from 1.908 to 2.181 kg C m^{-2} during the period from 1989 to 2003 (Yang and Guan 2008). The factors mean biomass density (MBD), mean ratio (MR), and continuous biomass expansion factor (BEF) were applied to forest inventory data to estimate China's forest biomass carbon stocks and their changes from 1984 to 2003. In terms of the BEF, carbon stocks of forest biomass increased from 4.0 to 5.9 Pg C. According to the MR, the carbon stocks (CS) rose from 4.2 to 6.2 Pg, and according to the MBD, the carbon stocks grew from 5.7 to 7.7 Pg (Guo et al. 2010). A study based on seven forest inventories from 1973 to 2008 indicated that total biomass carbon stock (CS) for all forest types increased by 65% from 1973 to 2008 and recently reached 8.12 Pg in China (Zhang et al. 2013).

A satellite-based approach suggested that the averaged forest biomass CS and CD in northeastern China were respectively 2.10 Pg (1 Pg = 10^{15} g) and 4.465 kg m^{-2} between 1982 and 1999. The forest biomass CS increased by 7% with an annual rate of 0.0082 Pg (Tan et al. 2007). It was highlighted that the vegetation restoration in the subalpine coniferous forest was a large carbon sink in the western Sichuan province of China (Xian et al. 2009). The total forest biomass of China averaged 5.79 Pg C between 1981 and 1999, with an average biomass density of 4.531 kg C m-2. The total forest biomass CS increased from 5.62 Pg in the early 1980s to 5.99 Pg by the end of the 1990s, giving a total increase of 0.37 Pg and an annual sequestration rate of 19 kg yr^{-1} (Piao et al. 2005). China's terrestrial ecosystems were a net carbon sink in the range of 0.19–0.26 Pg carbon per year and absorbed 28–37% of its cumulated fossil carbon emissions during the 1980s and 1990s. Northeast China is a net source of CO_2 due to overharvesting and forest degradation while southern China accounts for more than 65% of the carbon sink, which can be attributed to regional climate change, large-scale plantation programs initiated in the 1980s, and shrub recovery (Piao et al. 2009).

18.3.1 Data

18.3.1.1 Data Produced Using the National Forest Inventory Database

The national forest inventory database consists of seven datasets obtained from inventory data measured from 1984 to 1988 (termed as P1), 1989 to 1993 (P2), 1994 to 1998 (P3), 1999 to 2003 (P4), 2004 to 2008 (P5), 2009 to 2013 (P6), and 2014 to 2018 (P7). The data included 160,000 permanent sample plots and 90,000 temporary sample plots scattered over the whole land of China. The biomass density of each forest type in each province was calculated using linear relationships between a biomass expansion factor (BEF) and timber volume (Table 18.1):

$$BEF_{i,j} = a_i + \frac{b_i}{V_{i,j}} \tag{18.16}$$

The carbon density of each forest type in each province was calculated by multiplying biomass density by a carbon factor (CF) (Table 18.2). The CS by forest type in individual provinces was calculated by multiplying forest type area by CD. The total CS in China was the sum of the CS of all forest types in the 31 provinces of China, excluding Taiwan, Hong Kong, and Macao.

TABLE 18.1
Parameters Used to Calculate the Biomass Expansion Factor (BEF) for Different Forest Types in China (From Fang et al. 2007)

Forest Type	*a* (kg/m³)	*b* (kg/m²)	Number of Samples	R^2
Abies, Picea	551.9	4.8861	24	0.78
Tsuga, Cryptomeria, Keteleeria	349.1	3.9816	30	0.79
Larix	609.6	3.3806	34	0.82
P. koraiensis	572.3	1.6489	22	0.93
P. sylyestris var. mongolica	1,112	0.2695	15	0.85
P. tabulaefomis	869	0.9121	112	0.91
P. armandii	585.6	1.8744	9	0.91
P. massoniana, P. yunnanensis	503.4	2.0547	52	0.87
Cunninghamialanceolata	465.2	1.9141	90	0.94
Cypress	889.3	0.7397	19	0.87
Other pines and conifer forests	529.2	2.5087	19	0.86
Deciduous oaks	1,145.3	0.8547	12	0.98
Betula	1,068.7	1.0237	9	0.7
Mixed deciduous and Sassafras	978.8	0.5376	35	0.93
Eucalyptus	887.3	0.4554	20	0.8
Casuarina	744.1	3.2377	10	0.95
Populus	496.9	2.6973	13	0.92
Lucidophyllous forests	929.2	0.6494	24	0.83
Nonmerchantable woods	1,178.3	0.2559	17	0.95
Mixed conifer and deciduous	813.6	1.8466	10	0.99
Tropical forests	797.5	0.042	18	0.87

TABLE 18.2
Carbon Factor (CF) for Every Forest Type in China (From Li and Lei 2010)

Forest Type	CF	Forest Type	CF	Forest Type	CF
Pinuskoraiensis	0.5113	*Pinusyunnanensis*	0.5113	*Tilia*	0.4392
Abiesfabri	0.4999	*Pinuskesiya* var. langbianensis	0.5224	*Sassafras tzumu*	0.4848
Piceaasperata	0.5208	*Pinusdensata*	0.5009	*Eucalyptus robusta* Smith	0.5253
Tsugachinensis	0.5022	*Cunninghamialanceolata*	0.5201	*Casuarinaequisetifolia*	0.4980
Cupressusfunebris	0.5034	*Cryptomeriafortunei*	0.5235	*Populus*	0.4956
Larixgmelinii	0.5211	Metasequoiaglyptostroboides	0.5013	*Firmiana*	0.4695
*Pinussylvestris*var. mongolica	0.5223	Coniferous mixed forest	0.5101	Nonmerchantable woods	0.4834
Pinusdensiflora	0.5141	Broad-leaved and coniferous mixed forest	0.4978	Broad-leaved mixed forest	0.4900
Pinusthunbergii	0.5146	*Fraxinusmandschurica, Juglansmandshurica, Phellodendronamurense*	0.4827	Coppice	0.5000
Pinustabuliformis	0.5207	*Cinnamomumcamphora*	0.4916		
Pinusarmandii	0.5225	*Phoebe zhennan*	0.5030		
Keteleeriafortunei	0.4997	Oaks	0.5004		
Pinusmassoniana	0.4596	*Betula*	0.4914		

The following formulations were used to calculate the forest CS in China:

$$TCS = \sum_{i=1}^{M}\sum_{j=1}^{N} A_{i,j} \cdot BCD_{i,j} \cdot 10^{-12} \tag{18.17}$$

$$BCD_{i,j} = W_{i,j} \cdot CF_i \tag{18.18}$$

$$W_{i,j} = BEF_i \cdot V_{i,j} \tag{18.19}$$

where,TCS is the total forest carbon stocks of China (Pg); $BCD_{i,j}$ is the biomass carbon density of the i_{th} forest type in the j_{th} province, area weighted by mean forest carbon stocks (kg/m^2); $A_{i,j}$ is the area of the i_{th} forest type in the j_{th} province (m^2); M and N are respectively the number of forest types and number of provinces in China; $W_{i,j}$ is the area weighted mean forest biomass of the i_{th} forest type in the j_{th} province (kg m^{-2}); CF_i is the carbon factor of the i_{th} forest type; $V_{i,j}$ is the area weighted mean timber volume of the i_{th} forest type in the j_{th} province (m^3 m^{-2}); BEF_i is the biomass expansion factor of the i_{th} forest type (kg m^{-3}); a_i (kg m^{-3}) and b_i (kg m^{-2}) are constants for the i_{th} forest type to be simulated.

The CF_i value for coniferous mixed forests is an average of CF_i values for all coniferous forest types. For broad-leaved mixed forests and broad-leaved and coniferous mixed forests, the CF_i values were the averages of CF_i values for broad-leaved mixed forests and broad-leaved and coniferous forests, respectively.

18.3.1.2 Data Produced Using a Satellite-Based Approach (SBA)

The satellite data consisted of the Normalized Difference Vegetation Index (NDVI) from the Earth Observation System's moderate-resolution imaging spectroradiometer (EOS MODIS) at a spatial resolution of 1 × 1 km and 1-month interval. The spatial distribution map of China forests was obtained from the Vegetation Map of China published by the Institute of Botany, Chinese Academy of Sciences, in 2000. The carbon densities from forest inventory data were matched with NDVI data through the spatial distribution map of China forests.

The biomass carbon density was closely related to latitude, longitude, and the maximum value of the monthly averaged NDVI values during periods of national forest inventories, such as from 2004 to 2008 (Piao et al. 2005), i.e.,

$$\begin{aligned} BCD_j = {} & 93.351\ln(NDVI_j) - 2.96Lat_j - 21.388Lon_j \\ & + 0.047Lat_j^{\,2} + 0.091Lon_j^{\,2} + 1339.03 \end{aligned} \tag{18.20}$$

where, $NDVI_j$ is the mean value of the maximum values of the monthly averaged NDVI values in a period of the national forest inventory in the j_{th} province; Lat_j and Lon_j are latitude and longitude of the center of the j_{th} province, respectively. The coefficient of correlation was 0.91 ($P<0.001$).

18.3.2 Validation

Cross-validation included four steps: (i) 5% of the control points of each forest type in each province were removed for validation prior to model creation; (ii) the spatial distribution of average forest CS in China from 2004 to 2008 was simulated at a spatial resolution of 5 × 5 km using the remaining 95% of the control points; (iii) mean absolute error (MAE) and mean relative error (MRE) were calculated using the 5% validation set; and (iv) the 5% validation set was returned to the pool of available stations for the next iteration, and another 5% validation set was removed. This process

was repeated until all of the control points were used for validation at least one time, and the simulation error statistics for each control point could be calculated.

The MAE and MRE were respectively formulated as,

$$MAE = \frac{1}{n}\sum_{i}^{n}\left|o_i - s_i\right| \tag{18.21}$$

$$MRE = \frac{MAE}{\frac{1}{n}\sum_{i}^{n}\left|o_i\right|} \tag{18.22}$$

where,o_i represents forest carbon stocks at the i_{th} control point for validation, s_i is the simulated value at the i_{th} control point for validation, and n_i is the total number of control points for validation.

The cross-validation results indicated (Figure 18.1) that MAEs from YUE-HASM and SBA were 1.303 kg·m^{-2} and 1.919 kg·m^{-2}, respectively, while MREs were 33% and 49%. MRE for YUE-HASM was 16% lower than MRE for SBA. A regression analysis showed that the simulated CS using YUE-HASM was related to the observed CS more closely compared with the results obtained using SBA. The correlation coefficient between the YUE-HASM results and the observed data was 0.99 while the coefficient between the SBA results and the observed data was 0.89 (Figure 18.2). In other words, YUE-HASM had a much higher accuracy than SBA.

The annual mean carbon stock (AMCS) predicted using YUE-HASM for all forest types in China was 7.08 Pg between 2004 and 2008, of which AMCS for coniferous, broadleaf, and mixed forests were respectively 2.74, 3.95, and 0.39 Pg, respectively (Table 18.3). The annual mean carbon density (AMCD) was 4.55 kg/m^2 between 2004 and 2008, of which AMCD for coniferous forests, broadleaf forests, and mixed forests were 4.351, 4.742, and 4.198 kg/m^2, respectively. SBA underestimated AMCD for coniferous and broadleaf forests but overestimated AMCD for mixed forests.

18.3.3 Results

A zoning system dividing the land mass of China into nine regions with similar temperature, precipitation, and soil regimes was adopted to facilitate the analysis of the changes in forest carbon storage among different locations (Zhou et al. 1981). The nine regions were respectively termed as R_i (i=1 to 9) (Figure 18.3). The simulation results using YUE-HASM indicated that about 90% of AMCS was distributed in the R3, R5, R6, R7, and R9 regions, which accounted for 28.6%, 27.9%, 15.3%, 11.7%, and 6.1%, respectively, in the 2004–2008 period. The three largest AMCDs were in the regions R5 (Tibet plateau), R2 (arid area), and R3 (northeastern China), and the two smallest in R8 and R9 (Table 18.4 and Figure 18.1b). Results by forest types indicated that the AMCD of evergreen forests was greater than the AMCD for deciduous forests (Table 18.5). AMCS for evergreen coniferous forests had the highest proportion, accounting for 33.05%; which was followed by deciduous broad-leaved forests, accounting for 29.8%; and evergreen broad-leaved forests, accounting for 25.99% (Table 18.5). The broad-leaved and coniferous mixed forests and the deciduous coniferous forests accounted for the first two smallest proportions of the total CS, respectively 5.51% and 5.65%.

YUE-HASM simulation results indicated that AMCS rose 4.22 Pg from P1 to P7, mainly because of the increase in AMCD and the expansion of forest area (Table 18.6). AMCD increased by 1.035 kg m^{-2} from P1 to P7. The forest area increased by 0.3458 million km^2 in the same period. The regression analysis of the patterns of increase in AMCS, AMCD, and forest area resulted in significant relationships.

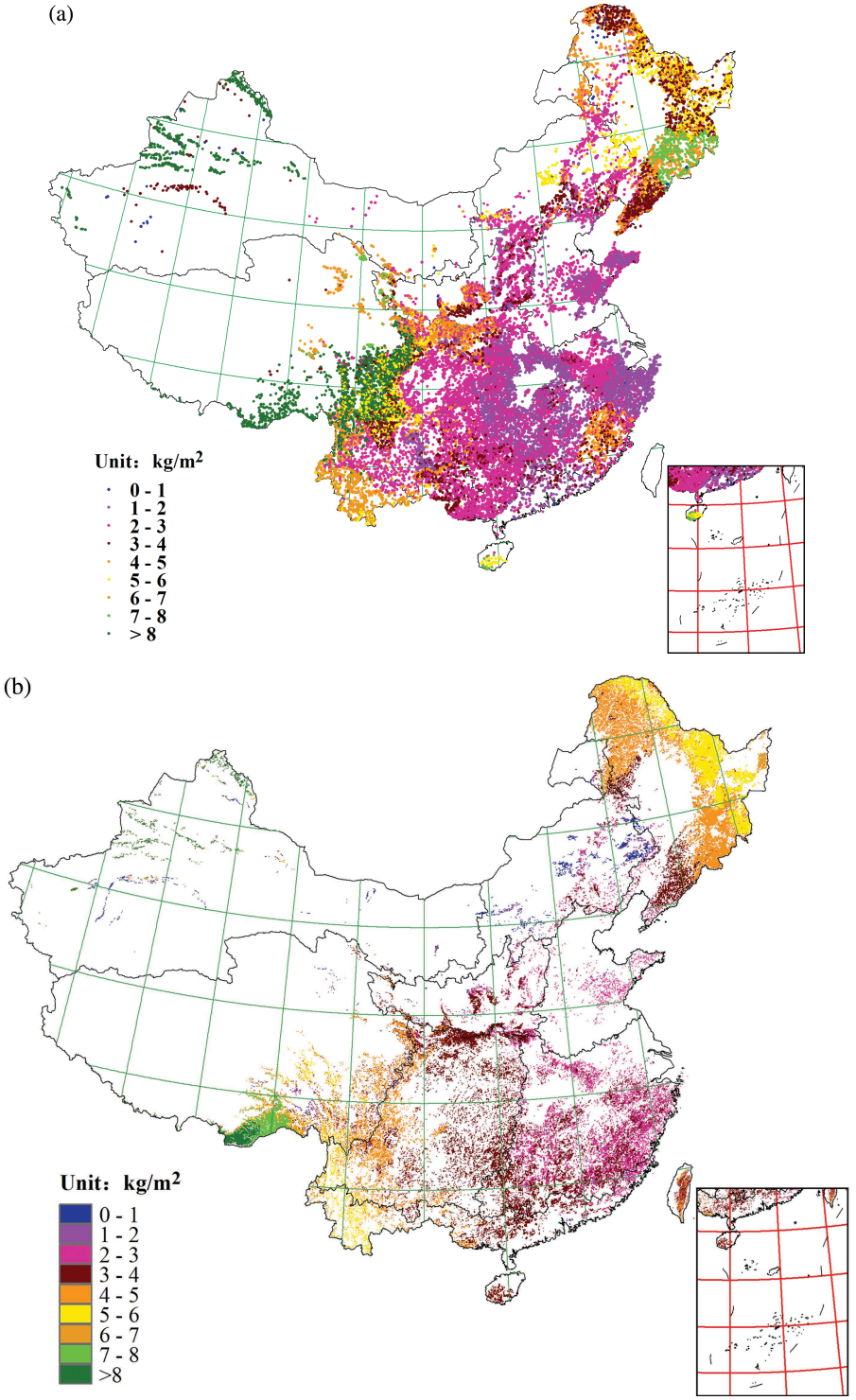

FIGURE 18.1 Spatial distribution of annual mean carbon density (AMCD) in forests during the 2004–2008 period in China: (a) observed, (b) using a satellite-based approach, and (c) YUE-HASM earth surface modeling methods.

(*Continued*)

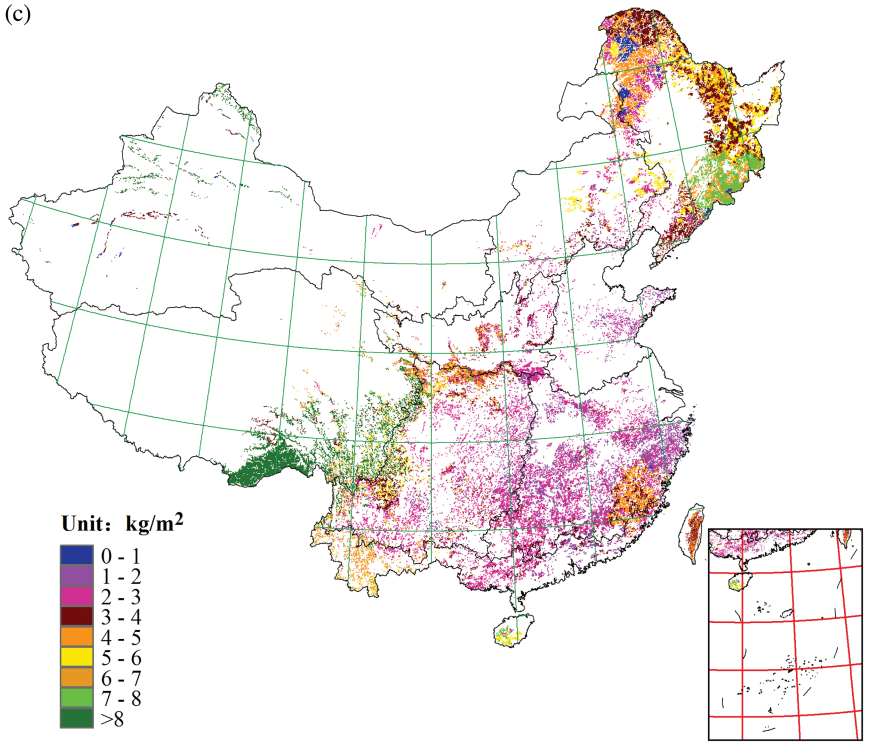

FIGURE 18.1 (*Continued*)

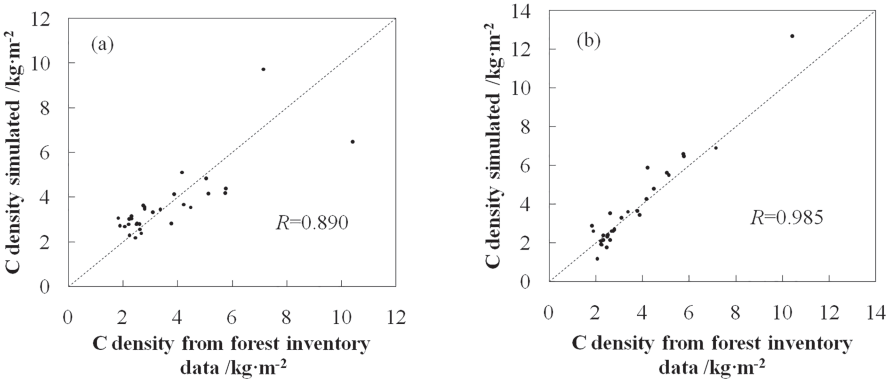

FIGURE 18.2 Comparison between observed and simulated results for annual mean carbon density (AMCD) in the 31 provinces obtained by (a) satellite-based approach and (b) YUE-HASM earth surface modeling methods.

TABLE 18.3
Comparison of Annual Mean Carbon Stocks (AMCS) and Annual Mean Carbon Density (AMCD) Using a Satellite-Based Approach (SBA) and YUE-HASM for Different Forest Types in China

	SBA		YUE-HASM	
Forest Type	**AMCS (Pg)**	**AMCD (kg/m²)**	**AMCS (Pg)**	**AMCD (kg/m²)**
Coniferous forests	2.48	3.937	2.74	4.351
Mixed forests	0.46	4.926	0.39	4.198
Broadleaf forests	3.61	4.338	3.95	4.742
Total	6.55		7.08	

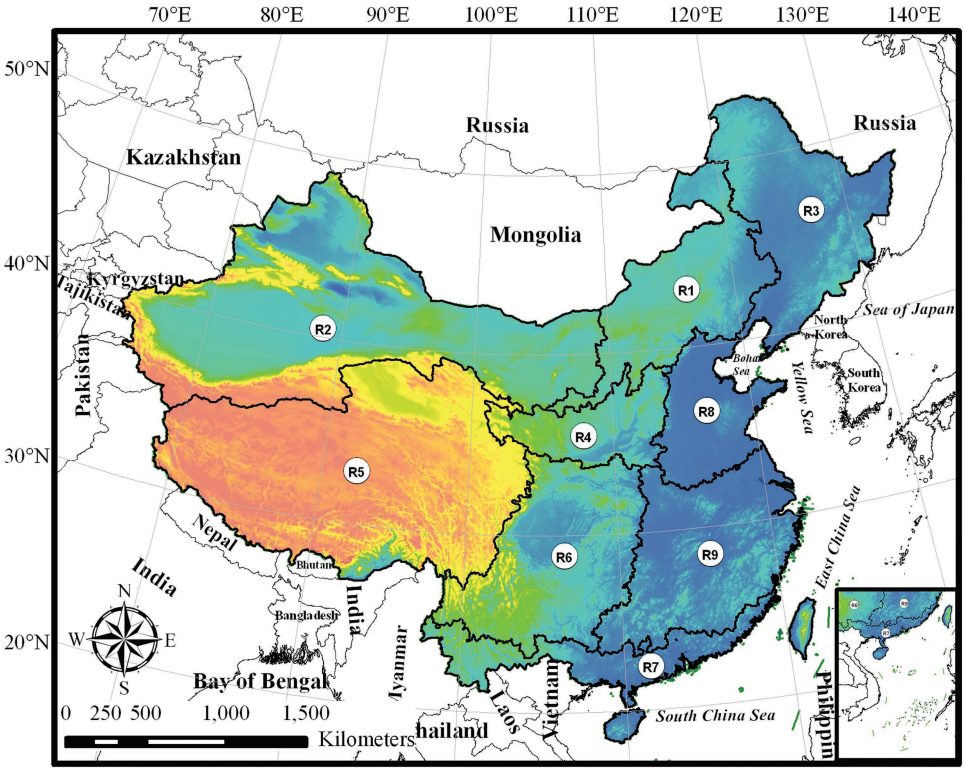

FIGURE 18.3 The nine regions of China characterized by similar temperature and precipitation conditions and soil regimes. R1 represents Inner Mongolia and the area along the Great Wall, R2 represents Arid area of China, R3 represents Northeastern China, R4 represents Loess plateau, R5 represents Tibet plateau, R6 represents Southwest China, R7 represents Southern China, R8 represents Huang-Huai-Hai River Plain, and R9 represents Middle and lower reaches of Yangtze River Basin.

TABLE 18.4
Annual Mean Carbon Stocks (AMCS) and Annual Mean Carbon Density (AMCD) for Forests in the Nine Regions of China from 2014 to 2018 and from 1984 to 1988

	2014–2018			1984–1988		CS Accumulation Rate
Regions	AMCD ($kg \cdot m^{-2}$)	AMCS (Pg)	Percentage (%)	AMCD ($kg \cdot m^{-2}$)	AMCS (Pg)	($Pg \cdot year^{-1}$)
R1	4.946	0.43	4.75	2.666	0.16	0.0090
R2	7.250	0.26	2.87	6.358	0.15	0.0037
R3	5.122	2.67	29.47	4.493	1.59	0.0360
R4	3.751	0.25	2.76	3.035	0.13	0.0040
R5	11.079	2.45	27.04	6.718	0.99	0.0487
R6	4.204	1.35	14.9	3.734	0.82	0.0177
R7	3.992	0.52	5.74	3.643	0.36	0.0053
R8	2.370	0.08	0.88	1.515	0.03	0.0017
R9	2.736	1.05	11.59	2.358	0.62	0.0143
Total		9.06	100		4.84	0.1407

TABLE 18.5
Annual Mean Carbon Density (AMCD) and Annual Mean Carbon Stocks (AMCS) for Different Forest Types in China from 2014 to 2018

Forest Types	AMCD ($kg\ m^{-2}$)	AMCS (Pg)	Percentage (%)
Deciduous coniferous forests	4.214	0.59	6.51
Evergreen coniferous forests	4.527	2.49	27.48
Broad-leaved and coniferous mixed forests	4.467	0.67	7.40
Deciduous broad-leaved forests	4.847	2.86	31.57
Evergreen broad-leaved forests	6.622	2.45	27.04
Total		9.06	100

TABLE 18.6
Annual Mean Carbon Stocks (AMCS) and Annual Mean Carbon Density (AMCD) of China in the Seven Study Periods (Excluding the Taiwan Province, Hong Kong, and Macao)

Periods	Area (million km^2)	AMCS (Pg)	AMCD ($kg\ m^{-2}$)
P1	1.2101	4.84	4.001
P2	1.2864	5.55	4.315
P3	1.2920	5.60	4.334
P4	1.4279	6.38	4.469
P5	1.5559	7.08	4.550
P6	1.6460	7.97	4.842
P7	1.7989	9.06	5.036

$$AMCS(t) = 0.6779t + 3.9286,\ R^2=0.96 \tag{18.23}$$

$$AMCD(t) = 0.1563t + 3.8817,\ R^2=0.95 \tag{18.24}$$

$$FA(t) = 0.0982t + 1.10668,\ R^2=0.96 \tag{18.25}$$

where, t corresponds to Pt, t = 1 to 7. $AMCS(t)$, $AMCD(t)$, and $FA(t)$ are respectively AMCS, AMCD, and forest area in the period of Pt.

Although AMCS increased in the nine regions from P1 to P7, it spatially varied over China, in concordance with forest distribution (Figure 18.4, Tables 18.4 and 18.7). In the regions R1 and R8, both AMCS and AMCD were characterized by a pattern of increase from P1. The smallest AMCS were obtained in R8, which accounted for only 0.88% of the total AMCS of China, and the smallest AMCD of 2.37 kg/m^2 in the period P7 as well as the lowest CS accumulation rate of 0.0017Pg·yr^{-1}. In R1, AMCS accounted for 4.75% of the total AMCS of China in the period P7; the CS accumulation rate was 0.0090 Pg·yr^{-1} on average.

The region R3 had the largest AMCS accounting for 29.47% of total AMCS of China in P7. The AMCS had a monotonically increasing trend since P1. The second largest AMCS appeared in the region R5. Its AMCS accounted for 27.04% of the total AMCS. It has the largest AMCD and the fastest CS accumulation rate of 0.0487 Pg year^{-1} (Table 18.7). In the regions R4 (loess plateau), R6, and R9, both AMCS and AMCD increased since P3. AMCS in R4, R6, and R9 accounted for 2.76%, 14.9%, and 11.59%, respectively, in the period P7. The CS accumulation rate was 0.0040, 0.0177, and 0.0143 Pg year-1. In R2, AMCS accounted for 2.87% in the period P7; AMCS and AMCD increased from the periods P4 to P7. The accumulation rate in CS was 0.0037 Pg year-1. In R7, AMCS accounted for 5.74%; AMCS and AMCD increased from the period P4 to P7. The CS accumulation rate was 0.0053 Pg year^{-1}.

In terms of forest types, evergreen broad-leaved forests had the fastest CS accumulation rate and the largest AMCD while deciduous broad-leaved forests had the biggest AMCS (Table 18.8). AMCS of broad-leaved forests increased during the seven periods while AMCS for evergreen broad-leaved forests increased from 0.63 to 2.45 Pg from P1 to P7, and it increased from 1.38 to 2.86 Pg in deciduous broad-leaved forests during the same period. Their patterns of increase had the following regression equations, respectively:

$$AMCS_1(t) = 0.305t + 0.3014,\ R^2=0.99 \tag{18.26}$$

$$AMCS_2(t) = 0.2539t + 0.9800,\ R^2=0.97 \tag{18.27}$$

where, t corresponds to Pt, t = 1 to 7; $AMCS_1(t)$ and $AMCS_2(t)$ are, respectively, AMCS for evergreen broad-leaved and deciduous broad-leaved forests in the period Pt.

AMCS for deciduous coniferous forests fluctuated among periods (Table 18.8). Evergreen coniferous and broad-leaved and coniferous mixed forests showed general patterns of increase in AMCS, which were formulated by the following regression equations,

$$AMCS_3(t) = 0.1521t + 1.5257,\ R^2=0.85 \tag{18.28}$$

$$AMCS_4(t) = 0.1046t - 0.1400,\ R^2=0.90 \tag{18.29}$$

where, t corresponds to Pt, t = 1 to 7; $AMCS_3(t)$ represents AMCS for evergreen coniferous forests in the period of Pt, and $AMCS_4(t)$ is AMCS for broad-leaved and coniferous mixed forest.

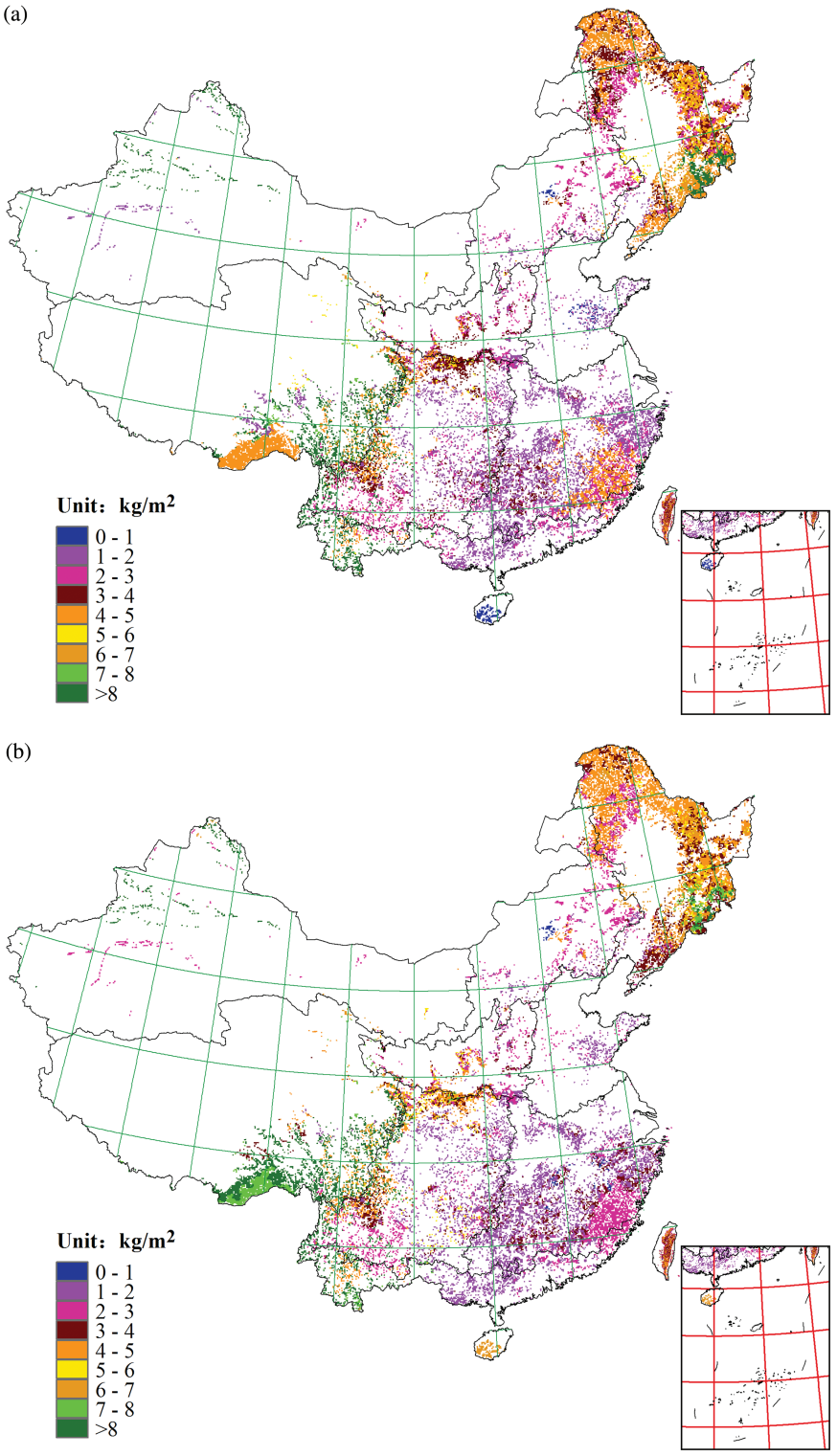

FIGURE 18.4 Spatial distribution of forest annual mean carbon density (AMCD) in China in the seven study periods: (a) 1984–1988 (P1), (b) 1989–1993 (P2), (c) 1994–1998 (P3), (d) 1999–2003 (P4), (e) 2004–2008 (P5), (f) 2009–2013 (P6), and (g) 2014–2018 (P7).

(*Continued*)

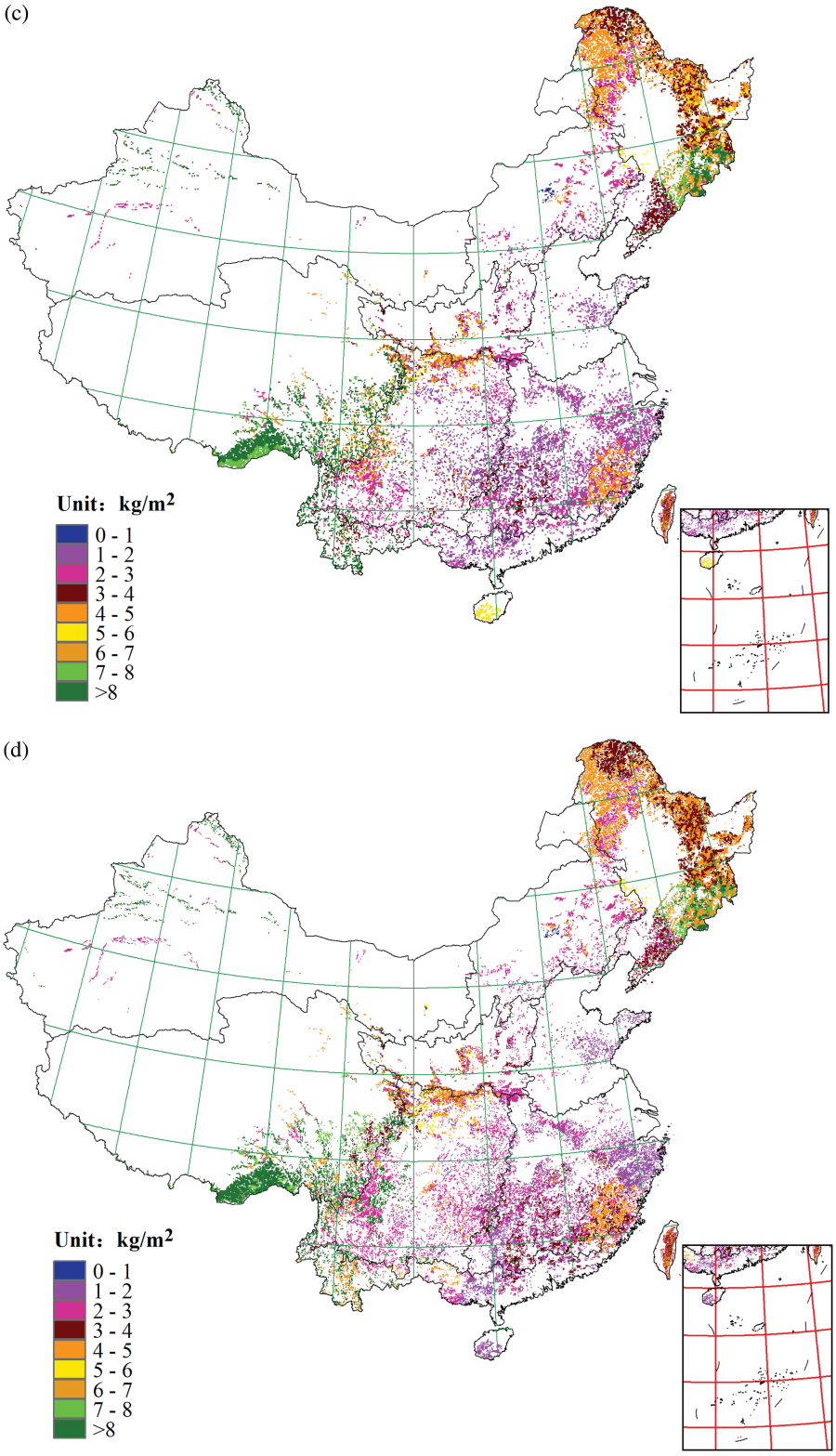

FIGURE 18.4 (*Continued*)

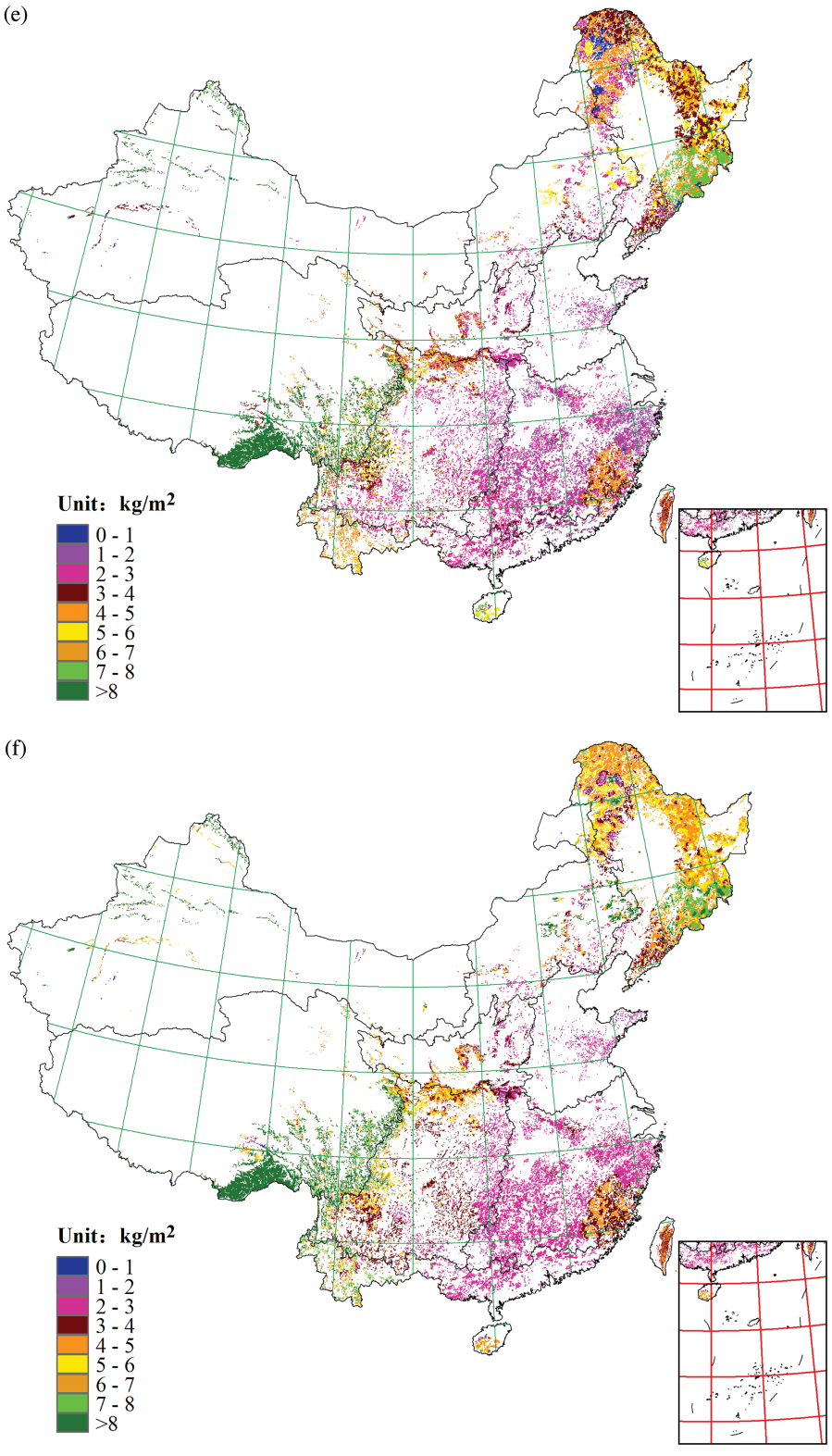

FIGURE 18.4 (*Continued*)

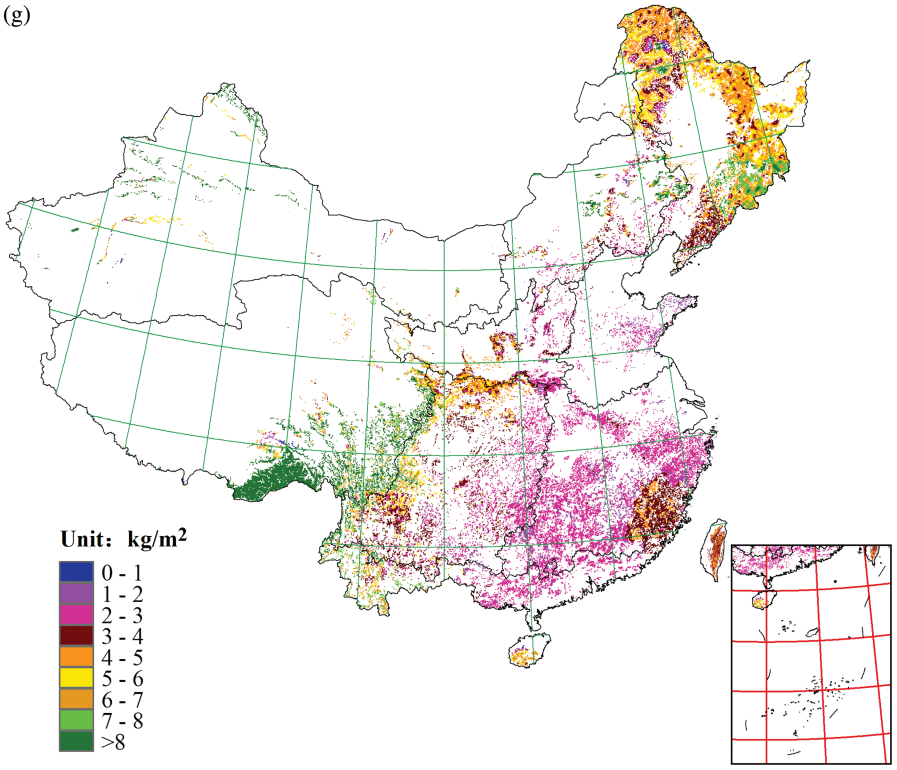

FIGURE 18.4 (*Continued*)

18.3.4 Discussion

Ground national forest inventory is able to accurately estimate forest carbon stocks with high temporal resolution using sample plots, but these sample plots are too sparse to satisfy the spatial simulation of carbon stocks with required accuracy. SBA can supply spatially continuous information about the surface of forest carbon stocks, which is impossible to obtain from ground-based investigations, but remote sensing description has considerable uncertainties. YUE-HASM overcame the shortcomings of the ground national forest inventory and SBA by fusing information about the details of the carbon stocks observed on the Earth surface and the change in the carbon surface observed from outside the Earth surface. The cross-validation demonstrates that YUE-HASM is 16% more accurate than the SBA.

In terms of the results obtained from YUE-HASM, forest carbon stocks of China increased by 4.42 Pg from 1984 to 2018. The Grain for Green program made a great contribution to this carbon stock increase. This program aims at restoring the forests and grasslands of China to prevent soil erosion. Program designers made the steepness of slopes, one of the main criteria on which plots were selected, for inclusion into the Grain for Green program (Xu et al. 2006). The steepness criterion means that the program targets land with a slope greater than 25°.

The Grain for Green program was divided into three phases: the experimental phase from 1999 to 2001, the construction phase from 2002 to 2010, and the consolidation phase from 2011 to 2020. By the end of 2001, 1.206 million hectares of farmland had been converted into forestland or grassland, and 1.097 million hectares of barren land had been afforested. Before 2011, 14.667 million hectares of farmland would have been converted to forestland or grassland, for which almost all

TABLE 18.7
Annual Mean Carbon Stocks (AMCS) and Annual Mean Carbon Density (AMCD) for Nine Chinese Regions in the Seven Study Periods

Forest types	P1		P2		P3		P4		P5		P6		P7	
	AMCS (Pg)	AMCD (kg m^{-2})	AMCS (Pg)	AMCD (kg m^{-2})	AMCS (Pg)	AMCD (kg m^{-2})	AMCS (Pg)	AMCD (kg m^{-2})	AMCS (Pg)	AMCD (kg m^{-2})	AMCS (Pg)	AMCD (kg m^{-2})	AMCS (Pg)	AMCD (kg m^{-2})
R1	0.16	2.67	0.17	2.71	0.17	2.88	0.2	2.98	0.27	3.57	0.38	4.77	0.43	4.95
R2	0.15	6.36	0.16	6.27	0.15	6.25	0.18	6.23	0.2	6.35	0.24	7.12	0.26	7.25
R3	1.59	4.49	1.64	4.42	1.64	4.5	1.77	4.43	1.98	4.37	2.34	4.91	2.67	5.12
R4	0.13	3.04	0.15	3.23	0.14	3.13	0.16	3.15	0.19	3.25	0.22	3.55	0.25	3.75
R5	0.99	6.72	1.57	10.15	1.64	10.83	1.94	11.49	2.03	10.53	2.21	10.92	2.45	11.08
R6	0.82	3.73	0.87	3.78	0.82	3.66	0.96	3.88	1.09	3.9	1.18	4.01	1.35	4.2
R7	0.36	3.64	0.39	3.79	0.37	3.66	0.4	3.54	0.44	3.87	0.45	3.81	0.52	3.99
R8	0.03	1.52	0.04	1.64	0.04	1.89	0.05	1.89	0.06	2.16	0.06	2.18	0.08	2.37
R9	0.62	2.36	0.56	2.05	0.62	2.3	0.73	2.51	0.83	2.49	0.89	2.53	1.05	2.74

TABLE 18.8
Annual Mean Carbon Stocks (AMCS) and Annual Mean Carbon Density (AMCD) for All Forest Types during the Seven Study Periods

Forest Types	P1		P2		P3		P4		P5		P6		P7	
	AMCS (Pg)	AMCD (kg m^{-2})	AMCS (Pg)	AMCD (kg m^{-2})	AMCS (Pg)	AMCD (kg m^{-2})	AMCS (Pg)	AMCD (kg m^{-2})	AMCS (Pg)	AMCD (kg m^{-2})	AMCS (Pg)	AMCD (kg m^{-2})	AMCS (Pg)	AMCD (kg m^{-2})
Deciduous coniferous forests	0.41	4.35	0.39	4.28	0.44	4.2	0.47	4.37	0.4	3.77	0.46	3.83	0.59	4.21
Evergreen coniferous forests	1.5	3.81	1.8	4.13	2.23	4.09	2.19	4.4	2.34	4.47	2.39	4.51	2.49	4.53
Broad-leaved and coniferous mixed forests	0.06	3.08	0.09	3.75	0.07	3.03	0.19	5.18	0.39	4.2	0.48	4.36	0.67	4.47
Deciduous broad-leaved forests	1.38	3.75	1.44	3.77	1.66	3.87	1.97	3.89	2.11	3.93	2.55	4.55	2.86	4.85
Evergreen broad-leaved forests	0.63	4.35	0.87	5.65	1.2	6.35	1.57	7.49	1.84	6.22	2.09	6.33	2.45	6.62

TABLE 18.9
Areas of Converted Farmlands and Afforested Barren Lands in the Grain for Green Program in China (Million Hectares)

Year	Converted Farmlands	Afforestation on Bare Lands	Total
1999	0.381	0.066	0.448
2000	0.405	0.468	0.872
2001	0.420	0.563	0.983
2002	2.647	3.082	5.729
2003	3.367	3.767	7.133
2004	0.667	3.333	4.000
2005	1.114	1.321	2.435
1999–2010	14.667	17.333	32

farmland with a slope more than 25° would have been converted, and 2.667 million hectares of cultivated desertification land have been converted to grassland; 17.333 million hectares of barren land would have been afforested. During the consolidation phase, scientific management of the converted land and afforestation land will be strengthened to keep the achievement of the Grain for Green program, for which 72.933 billion kg of grains and 11.515 billion of RMB have been planned (Li 2006).

In 1999, the pilot program was first experimented in three provinces, Gansu, Shaanxi and Sichuan; 0.381 million hectares of farmland were converted into forestland, and 0.066 million hectares of barren land were afforested. In 2000, the experimental area was expanded to 17 provinces; the converted farmland and the afforested barren land were respectively 0.41 million hectares and 0.449 million hectares. In 2001, 20 provinces were involved in the experiment; 0.42 million hectares of farmland were converted into forestland, and 0.563 million hectares of barren land were afforested (Table 18.9). In 2002, the Grain for Green program was overall launched in China. By 2005, 9.001 million hectares had been withdrawn from farmland and planted with trees or converted to permanent grassland.

REFERENCES

Ahlberg, J.H., E.N. Nilson and J.L. Walsh. 1967. *The theory of splines and their application*. New York: Academic Press.

Baffetta F, P. Corona and L. Fattorini. 2012. A matching procedure to improve k-NN estimation of forest attribute maps. *For. Ecol. Manage*. 272:35–50.

Bengtsson, B.E. and S. Nordbeck. 1964. Construction of isarithms and isarithmic maps by computers. *BIT* 4:87–105.

Costanza, R. 1989. Model goodness of fit: A multiple resolution procedure. *Ecol. Modell*. 47:199–215.

Costanza, R. and T. Maxwell. 1991. Spatial ecosystem modeling using parallel processors. *Ecol. Modell*. 58:159–183.

Costanza, R., F.H. Sklar, and M.L. White. 1990. Modeling costal landscape dynamics. *BioScience* 40(2):91–107.

Deichmann, U. 1996. *A review of spatial population database design and modeling*. Technical Report 96–3, National Center for Geographic Information and Analysis, USA.

Deng H.B., P. Zheng, T.X. Liu, et al. 2011. Forest ecosystem services and eco-compensation mechanisms in China. *Environ. Manage*. 48:1079–1085.

Fang, J.Y., Z.D. Guo, S.L. Piao, et al. 2007. Terrestrial vegetation carbon sinks in China, 1981–2000. *Sci. China Ser. D. Earth Sci*. 50:1341–1350.

Friend, A.D. 1998. Parameterisation of a global daily weather generator for terrestrial ecosystem modeling. *Ecol. Modell*. 109:121–140.

Gao, Q. 1996. Dynamic modeling of ecosystems with spatial heterogeneity: A structured approach implemented in windows environment. *Ecol. Modell*. 85:241–252.

Guo, Z., J. Pang, Y. Pan, et al. 2010. Inventory-based estimates of forest biomass carbon stocks in China: A comparison of three methods. *For. Ecol. Manage*. 269:1225–1231.

Haber, W. 2021. Eco-environmental surface modelling requires integration of both extrinsic and intrinsic informations. *Sci China Earth Sci*. 64:185-186.

Haxeltine, A. and I.C. Prentice. 1996. BIOME3: An equilibrium terrestrial biosphere model based on ecophysiological constraints, resource availability, and competition among plant functional types. *Global Biogeochem. Cycles*10:693–710.

Ji, W. and C. Jeske. 2000. Spatial modeling of the geographic distribution of wildlife populations: A case study in the lower Mississippi River region. *Ecol. Modell*. 132:95–104.

Kleijnen, J.P.C. 2009. Kriging metamodeling in simulation: A review. *Eur. J. Oper. Res*. 192:707–716.

Kleijnen, J.P.C. and W.C.M. van Beers. 2005. Robustness of kriging when interpolating in random simulation with heterogeneous variances: Some experiments. *Eur. J. Oper. Res*. 165(3):826–834.

Krige, D.G. 1951. A statistical approach to some basic mine valuation problems on the Witwatersrand. *J. Chem. Metall. Min. Soc. S. Afr*. 52:119–139.

Legendre, L. and P. Legendre. 1983. *Numerical ecology*. Amsterdam: Elsevier Scientific Pul. Co.

Li, S.D. 2006. *Research on the optimized models of the conversion of farmland to forests in China*. Beijing: China Environmental Science Press (in Chinese).

Li, H. and Y.C. Lei. 2010. *Estimation and evaluation of forest biomass carbon storage in China*. Beijing: China Forestry Press (in Chinese).

Lo, C.P. and A.K.W. Yeung. 2002. *Concepts and techniques of geographic information systems*. Upper Saddle River, NJ: Prentice-Hall.

Long, G.E. 1980. Surface approximation: A deterministic approach to modeling spatially variable systems. *Ecol. Modell*. 8:333–343.

Magnussen, S., E. Naesset, and M.A. Wulder. 2007. Efficient multi-resolution spatial predictions for large data arrays. *Remote Sens. Environ*. 109:451–463.

Martin, D. and I. Bracken. 1991. Techniques for modeling population-related raster databases. *Environ. Plan*. 23:1069–1075.

Ni, J. 2013. Carbon storage in Chinese terrestrial ecosystems: approaching a more accurate estimate. *Clim. Change* 119:905–917.

Oliver, M.A. and R. Webster. 1990. Kringing: A method of interpolation for geographical information systems. *J. Geogr. Inf. Sci*. 4:313–332.

Perry, G.L.W. and N.J. Enright. 2002. Spatial modeling of landscape composition and pattern in a maquis-forest complex, Mont Do, New Caledonia. *Ecol. Modell*. 152:279–302.

Piao S.L., J.Y. Fang, B. Zhu, et al. 2005. Forest biomass carbon stocks in China over the past 2 decades: Estimation based on integrated inventory and satellite data. *J. Geophys. Res*. 110(G1). https://doi.org/10.1029/2005JG000014.

Piao S.L., J.Y. Fang, P. Ciais, et al. 2009. The carbon balance of terrestrial ecosystems in China. *Nature* 458:1009–1014.

Prentice I.C., L.O. Bengtsson, and C.U. Hammer. 2001. Interactions of climate change and the terrestrial biosphere. In *Geosphere-biosphere interactions and climate*, eds. L.O. Bengtsson and C.U. Hammer, pp. 176–195. Cambridge: Cambridge Books Online.

Quarteroni, A., R. Sacco, and F. Saleri. 2000. *Numerical mathematics*. New York: Springer.

Reich, R.M., C.D. Bonham, and K.L. Metzger. 1997. Modeling small-scale spatial interaction of shortgrass prairie species. *Ecol. Modell*. 101:163–174.

Schroeder, L.D. and D.L. Sjoquist. 1976. Investigation of population density gradients using trend surface analysis. *Land Econ*. 52:382–392.

Shepard, D. 1968. A two-dimensional interpolation function for irregularly-spaced data. In *Proceedings of the 1968 23rd ACM national conference*, pp. 517–524. New York: Association for Computing Machinery.

Shi, W.J., J.Y. Liu, Z.P. Du, et al. 2011. Surface modelling of soil properties based on land use information. *Geoderma* 162:347–357.

Shi, W.J., J.Y. Liu, Z.P. Du, et al. 2009. Surface modelling of soil ph. *Geoderma* 150(1–2):113–119.

Sklar, F.H., R. Costanza, and J.W. Day, Jr. 1985. Dynamic spatial simulation modeling of coastal wetland habitat succession. *Ecol. Modell*. 29:261–281.

Stott, J.P. 1977. Review of surface modeling. In *Proceedings of surface modeling by computer*, pp. 1–8. London: A conference jointly sponsored by the Royal Institution of Chartered Surveyors and the Institution of Civil Engineers, 1976.

Svirezhev, Y.M. 2002. Simple spatially distributed model of the global carbon cycle and its dynamic properties. *Ecol. Modell*. 155:53–69.

Tan, K., S.L. Piao, C.H. Peng, et al. 2007. Satellite-based estimation of biomass carbon stocks for northeast China's forests between 1982 and 1999. *For. Ecol. Manage*. 240:114–121.

Thurner, M., C. Beer, M. Santoro, et al. 2014. Carbon stock and density of northern boreal and temperate forests. *Glob. Ecol. Biogeogr*. 23:297–310.

Tse, R.O.C. and C. Gold. 2004. TIN meets CAD—Extending the TIN concept in GIS. *Future Gener. Comput. Syst*. 20:1171–1184.

Turner, M.G., R. Costanza, and F.H. Sklar. 1989. Methods to evaluate the performance of spatial simulation models. *Ecol. Modell*.48:1–18.

Wang, S., J.M. Chen, W.M. Ju, et al. 2007. Carbon sinks and sources in china's forests during 1901–2001. *J. Environ. Manage*. 85:524–537.

Watt, A. 2000. *3D Computer graphics*. New York: Addison-Wesley.

Wu, J.G. and S.A. Levin. 1997. A patch-based spatial modeling approach: conceptual framework and simulation scheme. *Ecol. Modell*.101:325–346.

Xian J.R., Y.B. Zhang, K.Y. Wang, et al. 2009. Carbon stock and its allocation in five forest ecosystems in the subalpine coniferous forest zone of western Sichuan province, southwest China. *Chin. J. Plant Ecol*. 33:283–290.

Xu ZG, J.T. Xu, X.Z. Deng, et al. 2006. Grain for Green versus grain: conflict between food security and conservation set-aside in China. *World Development* 34:130–148.

Yang, K. and D.S. Guan. 2008. Changes in forest biomass carbon stock in the Pearl River Delta between 1989 and 2003. *J. Environ. Sci*. 20:1439–1444.

Yang, Q.H., J.P. Snyder, and W.R. Tobler. 2000. *Map projection transformation*. New York, NY: Taylor &Francis.

Yue, T.X., C.C. Wu, Y. Liu, et al. 2023. HASM quantum machine learning. Science China-Earth *Sciences* 66(9):1937–1945.

Yue, T.X., Y. Liu, Z.P. Du, et al. 2022. Quantum machine learning of eco-environmental surfaces. *Sci. Bull*. 67:1031–1033.

Yue, T.X. 2011. *Surface Modelling: High accuracy and high speed methods*. New York: CRC Press.

Yue, T.X., S. Jorgensen, and G. Larocque. 2011. Progress in global ecological modelling. *Ecol. Modell*. 222:2172–2177.

Yue, T.X., C.F. Chen, and B.L. Li. 2010a. An adaptive method of high accuracy surface modeling and its application to simulating elevation surfaces. *Trans. GIS* 14:615–630.

Yue, T.X., D.J. Song, Z.P. Du, et al. 2010b. High-accuracy surface modelling and its application to dem generation. *Int. J. Remote Sens*. 31 2205–2226.

Yue, T.X., N. Zhao, H. Yang, et al. 2013b. A multi-grid method of high accuracy surface modeling and its validation. *Trans. GIS* 17:943–952.

Yue, T.X., N. Zhao, R.D. Ramsey, et al. 2013a. Climate change trend in China, with improved accuracy. *Clim. Change* 120:137–151.

Yue, T.X. and S.H. Wang. 2010. Adjustment computation of HASM: A high-accuracy and high-speed method. *Int. J. Geogr. Inf. Sci*. 24:1725–1743.

Yue, T.X., Y.A. Wang, and Z.M. Fan. 2009. Surface modeling of population distribution. In *Handbook of ecological modeling and informatics*, eds. S.E. j0rgensen, T.S. Chon, and F. Recknagel, pp. 71–98. Ashurst Lodge, Ashurst, Southampton S040 7AA, UK: WIT Press.

Yue, T.X., Z.M. Fan, and J.Y. Liu. 2007b. Scenarios of land cover in China. *Glob. Planet. Change* 55:317–342.

Yue, T.X., Z.P. Du, D.J. Song, et al. 2007a. Anew method of surface modeling and its application to DEM construction. *Geomorphology* 91:161–172.

Yue, T.X., Z.P. Du, and Y.J. Song. 2008. Ecological models: Spatial models and geographic information systems. In *Encyclopedia of ecology*, eds. S.E. Jorgensen and B. Fath, pp. 3315–3325. Oxford: Elsevier Limited.

Zhang C.H., W.M. Ju, J.M. Chen, et al. 2013. China's forest biomass carbon sink based on seven inventories from 1973 to 2008. *Clim. Change* 118:933–948.

Zhao, N. and T.X. Yue. 2014. A modification of HASM for interpolating precipitation in China. *Theor. Appl. Clim*. 116:273–285.

Zhao, C.Y., Z.G. Nan, and G.D. Cheng. 2005. Methods for modeling of temporal and spatial distribution of air temperature at landscape scale in the southern Qilian mountains, China. *Ecol. Modell*. 189:209–220.

Zhou L.S., H. Sun, Y.Q. Shen, et al. 1981. *Comprehensive agricultural planning of China*. Beijing: China Agricultural Press. (in Chinese)